CHEMISTRY OF MATERIALS

pubs.acs.org/cm

Article

Characterization of Chemisorbed Species and Active Adsorption Sites in Mg−Al Mixed Metal Oxides for High-Temperature CO_2 Capture

Alicia Lund, G. V. Manohara, Ah-Young Song, Kevin Maik Jablonka, Christopher P. Ireland, Li Anne Cheah, Berend Smit, Susana Garcia, and Jeffrey A. Reimer*

Cite This: *Chem. Mater.* 2022, 34, 3893−3901

Read Online

ACCESS | Metrics & More | Article Recommendations | Supporting Information

ABSTRACT: Mg−Al mixed metal oxides (MMOs), derived from the decomposition of layered double hydroxides (LDHs), have been purposed as adsorbents for CO_2 capture of industrial plant emissions. To aid in the design and optimization of these materials for CO_2 capture at 200 °C, we have used a combination of solid-state nuclear magnetic resonance (ssNMR) and density functional theory (DFT) to characterize the CO_2 gas sorption products and determine the various sorption sites in Mg−Al MMOs. A comparison of the DFT cluster calculations with the observed ^{13}C chemical shifts of the chemisorbed products indicates that mono- and bidentate carbonates are formed at the Mg−O sites with adjacent Al substitution of an Mg atom, while the bicarbonates are formed at Mg−OH sites without adjacent Al substitution. Quantitative ^{13}C NMR shows an increase in the relative amount of strongly basic sites, where the monodentate carbonate product is formed, with increasing Al/Mg molar ratios in the MMOs. This detailed understanding of the various basic Mg−O sites presented in MMOs and the formation of the carbonate, bidentate carbonate, and bicarbonate chemisorbed species yields new insights into the mechanism of CO_2 adsorption at 200 °C, which can further aid in the design and capture capacity optimization of the materials.

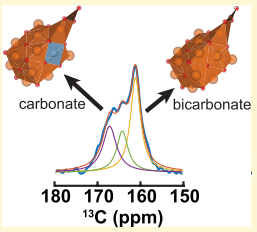

INTRODUCTION

Carbon dioxide capture, utilization, and storage (CCUS) are expected to play a key role in reducing atmospheric CO_2 and mitigating global warming.[1,2] Capturing CO_2 from industrial emissions is one of the several approaches toward this end.[3] Solid sorbents such as zeolites,[4] metal−organic frameworks (MOFs),[5,6] covalent organic frameworks (COFs),[7] mesoporous carbon,[8] and metal oxides[9] have all shown to be promising materials for CO_2 capture. Among the solid CO_2 sorbents, layered double hydroxide (LDH)-derived mixed metal oxides (MMOs) have shown promising CO_2 capture performance at the 200−500 °C temperature range that is associated with industrial emissions such as iron and steel plants.[10−13] LDHs derive their structure from the mineral brucite $Mg(OH)_2$, while partial isomorphous substitution of Mg^{2+} ions with higher valent cations (Al^{3+}, Fe^{3+} Ga^{3+}, etc.) leads to positively charged hydroxide layers. Charge-compensating anions and water molecules are incorporated into the interlayer galleries leading to the formation of the LDHs. LDHs are represented by the general formula $[M^{2+}_{1-x}M^{3+}_{x}(OH)_2]^{x+}(A^{-x/n})\cdot yH_2O$, where M^{2+} = Mg, Co, Ni, Ca, and Zn, M^{3+} = Al, Fe, and Ga, and A = anion (organic or inorganic ions), $0.15 \leq x \leq 0.33$ and $0.5 \leq y \leq 1.0$.[14] Due to their physicochemical properties, LDHs and LDH-derived MMOs have proved to be useful materials in various industrial applications including catalysis and sorption.[15−17] The substitution of Mg^{2+} with Al^{3+} also helps prevent the sintering of MgO. In the recent past, LDH-derived MMOs have gained prominence as CO_2 capture sorbents due to their high theoretical capture capacity, tolerance to moisture and hydrogen sulfide (H_2S), ease of preparation/handling, economical cost, and their environmentally friendly nature.[18−22] Interestingly, LDH-derived MMOs have shown unique CO_2 capture performance under both pre- and postcombustion conditions.[23] While the CO_2 capture properties are very promising, the performance of LDH-derived MMOs has yet to live up to the theoretical promise, with the typical measured CO_2 capture capacities being in the range of 0.05−1.39 mmol/g.[21] Moreover, MMOs have shown poor carbonation/regeneration cycling stability with the capture capacities decreasing by 30−50% over 10−20 cycles; overcoming these challenges has been the focus of much ongoing research.[21,24,25]

It is clear from this literature that a detailed atomistic understanding of the CO_2 capture process, including identification of the chemisorbed products, is needed to further drive the development of MMOs for increased capture capacity. Solid-state nuclear magnetic resonance (ssNMR)

Received: September 7, 2021
Revised: March 17, 2022
Published: April 21, 2022

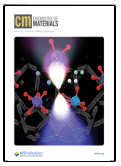

spectroscopy and, in particular, the chemical resolution of magic-angle spinning (MAS) has proven to be a powerful and well-established technique for discerning detailed molecular structure and elucidating the host−guest interactions in solid sorbent materials.[26−29] For example, combining multinuclear ssNMR and density functional theory (DFT) chemical shift calculations have been shown to give the detailed CO_2 chemisorption mechanisms of MOFs and porous solid sorbent materials.[30−32] Indeed, extensive NMR studies have been performed on precursor LDH materials[33] to gain structural information such as cation and anion ordering. Yet, few studies have focused on actual MMOs, likely due to their amorphous nature and the correspondingly broadened NMR linewidths vis-à-vis those with crystalline LDH parent materials. Exploiting multinuclear NMR techniques allows us to take advantage of the distance-dependent dipolar coupling between the NMR active guest nuclei and the host material nuclei; these data, combined with the DFT calculations of isotropic chemical shifts, afford insights into the local bonding configurations of MMOs and their interactions with sorbed CO_2. In this work, we seek to establish the chemisorbed products formed as a result of the interactions between CO_2 and Mg−Al MMOs and the effect of varying Al content on the chemisorbed products using an ex situ $^{13}CO_2$ dosing approach.[30] A detailed adsorption mechanism including whether the chemisorbed products are formed at the Mg or Al sites in the MMOs is also presented.

MATERIALS AND METHODS

Synthesis and Characterization. All the reagents $Mg(NO_3)_2{\cdot}6H_2O$, $Al(NO_3)_3{\cdot}9H_2O$, Na_2CO_3, NaOH, and nitric acid were purchased from Sigma Aldrich and used as received. Deionized water (18 MΩ cm resistivity, Millipore water purification system) was used for all the syntheses. Mg−Al−CO_3 LDH (with Al/Mg = 0.33, 0.25, 0.20, and 0.15) was synthesized by employing the coprecipitation method to yield LDH materials of the formula $[Mg_xAl_{1-x}(OH)_2]\ (CO_3)_{x/2}{\cdot}yH_2O$. Table 1 reports the actual synthesis formula of each LDH material determined from elemental analysis. In a typical experiment, 3 g of LDH was prepared by slow addition of an aqueous solution of $Mg(NO_3)_2{\cdot}6H_2O$ and $Al(NO_3)_3{\cdot}9H_2O$ into a 500 mL aqueous solution of Na_2CO_3 (3 times excess the stoichiometric amount of carbonate). The reaction medium was maintained at pH 10 by adding 1 N NaOH solution with the help of a Metrohm autotitrator, 907 Titrando. The reaction mixture was stirred continuously using a magnetic stirrer with the temperature being maintained at 70 °C. Once the addition of metal nitrates was complete, the resultant reaction mixture was aged in the mother liquor overnight. The resultant LDH was recovered by centrifugation followed by washing with 1500 mL of water. The product was dried overnight at 70 °C in an oven. The CO_2 capture studies were performed using a thermogravimetric analyzer (TA Instruments, Discovery series TGA 5500). For CO_2 capture studies, pristine LDHs were used instead of decomposed ones to avoid CO_2 contamination. Freshly prepared LDHs were loaded into a TGA pan and decomposed under an inert atmosphere (using 100 mL/min N_2, 4 h, 400 °C, 10 °C/min). Once the decomposition was complete, the temperature was brought back to 200 °C (10 °C/min) and the gas atmosphere was switched to CO_2 (for 2 h) to test the uptake capacity of the resultant MMOs under a 90% CO_2 atmosphere. For comparison, the CO_2 capture capacity of MgO derived from $Mg(OH)_2$ was carried out identical to the MMOs. To avoid experimental errors while calculating the CO_2 capture capacities, a blank experiment was conducted by loading an empty pan and the obtained mass gain was subtracted from the actual mass gain of all the MMOs. The MMOs were synthesized by decomposing the LDHs at 400 °C using a muffle furnace (ramp rate = 10 °C/min, residence time = 4 h) under N_2. $Mg(OH)_2$ was also calcined under the same conditions to form MgO as a metal oxide reference. After decomposing/calcination, the materials were stored in a glove box kept under an Ar atmosphere. Complete characterization including ICP-MS, XRD, and FTIR spectra and BET surface area determination of the LDHs and derived MMOs are provided in the Supporting Information (SI).

Table 1. Elemental Composition of the LDHs Obtained by the Coprecipitation Technique (ICP Analysis)

expected Al/Mg ratio	experimental Al/Mg ratio	approximate composition
0.33	0.31	$[Mg_{0.69}Al_{0.31}(OH)_2]\ (CO_3)_{0.155}{\cdot}0.53H_2O$
0.25	0.23	$[Mg_{0.77}Al_{0.23}(OH)_2]\ (CO_3)_{0.115}{\cdot}0.65H_2O$
0.20	0.18	$[Mg_{0.82}Al_{0.18}(OH)_2]\ (CO_3)_{0.09}{\cdot}0.73H_2O$
0.15	0.18	$[Mg_{0.82}Al_{0.18}(OH)_2]\ (CO_3)_{0.09}{\cdot}0.73H_2O$

NMR Characterization. Prior to CO_2 gas dosing, the samples were packed inside a glove box in a 4 or 3.2 mm zirconia rotor. Then the uncapped rotor was placed into a specialized ex situ gas dosing system[30] fitted with a tube furnace that allows for $^{13}CO_2$ dosing at 200 °C. Care was taken to ensure the calcined samples were not exposed to air, thus preventing the absorption of atmospheric water and/or CO_2. The uncapped rotors were evacuated for 30 min prior to gas dosing. While held at a constant temperature of 200 °C, the samples were dosed with 1 bar of $^{13}CO_2$ gas (Sigma-Aldrich Carbon-^{13}C dioxide <3 atom % ^{18}O, 99.0 atom % ^{13}C) and allowed to equilibrate for 1 h. The rotor was then cooled to 120 °C and the Kel-F cap was quickly placed on the rotor without exposing the dosed material to the atmosphere. The sealed 4 mm rotor was inserted into an 11.74 T magnet (500 MHz ^{1}H Larmor frequency, Avance I Bruker spectrometer) using a Bruker dual-channel CPMAS probe. The TRAPDOR measurements were performed using a 16.4 T magnet (700 MHz ^{1}H Larmor frequency, Bruker Avance I spectrometer) with a 3.2 mm Bruker triple channel ^{1}H/^{13}C/^{15}N probe. All NMR measurements were performed at room temperature with a MAS rate of 10 kHz. All spectral deconvolution, including quadrupolar and chemical shift parameters, were determined using the spectral fitting software Dmfit.[34]

A rotor synchronized DEPTH[35] pulse sequence was employed to remove the background ^{1}H signal and quantitate the ^{1}H spectrum, with a radio field (*rf*) strength of 57 kHz, and a recycle delay of 2 s, equivalent to $5T_1$. Quantitative ^{13}C measurements were performed using a single pulse with *rf* strength of 75 kHz and proton decoupling (50 kHz strength) during acquisition with a recycle delay of 600 s, equivalent to $5T_1$. The 1D ^{1}H−^{13}C cross polarization (CP) spectra were measured with a contact time of 2 ms, an *rf* strength of 70 kHz ^{1}H, a ramp 30 to 50 kHz ^{13}C *rf* field strength, and a ^{1}H decoupling power of 80 kHz during detection. The 2D ^{1}H−^{13}C heteronuclear correlation spectra were measured with a contact pulse of 200 μs to probe only the ^{1}H in spatial proximity to the chemisorbed $^{13}CO_2$ species. Frequency switched Lee−Goldberg decoupling was applied during the ^{1}H evolution period at 80 kHz *rf* strength.[36] Multiple quantum magic-angle spinning (MQMAS) ^{27}Al NMR measurements were also performed on the MMOs before and after gas dosing. An *rf* strength of 180 kHz for the ^{27}Al measurements was used. The quantitative single pulse measurements obtained using a small flip angle of 30 degrees to ensure NMR signal intensity was not affected by differences in quadrupolar coupling frequencies of the ^{27}Al environments. The *z*-filtered MQMAS sequence was used with a selective 90 pulse of 30 kHz *rf* strength.[37] Adamantane was used as an external reference for both the ^{1}H and ^{13}C chemical shifts and 0.1 M $Al(NO_3)_3$(aq) was used for the chemical shift and *rf* strength calibration of ^{27}Al. The TRAPDOR measurements were performed at a magnetic field strength of 16.4 T. Here the standard Hahn-echo sequence ($90-\tau-180-\tau$) was used to collect the rotor-

https://doi.org/10.1021/acs.chemmater.1c03101
Chem. Mater. 2022, 34, 3893−3901

synchronized ^{1}H echo and during the first τ period continuous wave ^{27}Al irradiation was applied at an *rf* strength of 160 kHz. At each subsequent step, τ was incremented by a multiple of the rotor period and the ^{1}H Hahn echo was recorded with and without ^{27}Al irradiation.

DFT Simulation Parameters. Density functional theory (DFT) calculations of isotropic chemical shifts were conducted to get insights into the local bonding configurations of MMOs and their interaction with sorbed CO_2. The starting structure for the simulation of the MMO cluster was a cubic MgO cluster as described in the literature.[38] The B3LYP hybrid functional with the double-valence double-zeta polarized basis set 6-31++G** was chosen as the hybrid functional and basis set as it is suitable for qualitative trends in MMO cluster calculations.[39,40] The simulations were orchestrated using the AiiDA workflow manager[41] and the DFT calculations were performed using Gaussian 16;[42] for convergence, the YQC algorithm was used. NMR shifts were calculated using the gauge-independent atomic orbital (GIAO) formalism.[43] The dimer trimethylaluminum was used as a reference for determining the chemical shift from the chemical shielding calculations. Chemical shifts are reported at $\delta_{iso} = \sigma_{ref} - \sigma_{iso}$.

RESULTS AND DISCUSSION

Chemisorption Mechanism. The direct ^{13}C NMR spectra of $^{13}CO_2$-dosed MMOs and MgO (Figure 1) present two

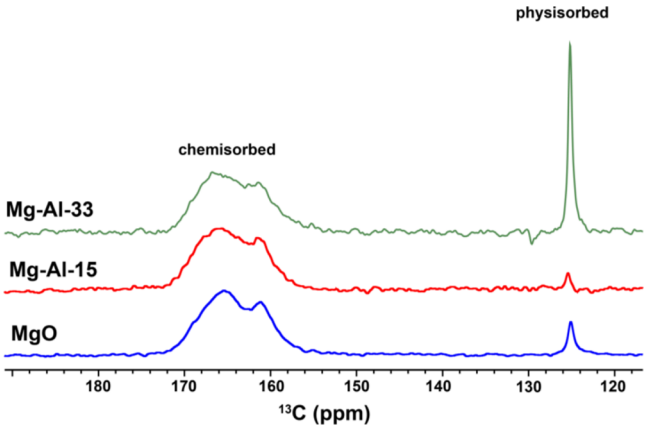

Figure 1. Direct ^{13}C spectrum of all MMO and MgO dosed with $^{13}CO_2$ at 1 bar and 200 °C. The direct ^{13}C excitation shows both physisorbed and chemisorbed CO_2.

distinct regions of observed ^{13}C chemical shifts. The peak at 125.1 ppm is assigned to physisorbed CO_2 as it agrees well with previously reported chemical shifts of physisorbed CO_2 in similar LDH and crystalline MgO materials.[44,45] The peaks in the region 160−170 ppm are assigned to chemisorbed carbonate and bicarbonate species in comparison to the known shifts of such compounds.[46−48]

Analysis of the integral in the quantitative ^{13}C NMR spectra shows that the chemisorbed CO_2 comprises 80−93% of the CO_2 adsorbed in the MMOs. The ^{1}H−^{13}C CP spectra of $^{13}CO_2$-dosed MMOs with Al content of Al/Mg = 0.15 and 0.33 denoted Mg−Al−15 and Mg−Al−33, respectively, and decomposed MgO are shown in Figure 2. The CPMAS spectrum measures the ^{13}C signal of those species that are strongly dipolar coupled to ^{1}H spins in the MMO framework and reveals only the chemisorbed species since the physisorbed CO_2 exhibits negligible ^{1}H dipolar coupling. In the 1D ^{13}C CPMAS spectra of all the dosed materials, three chemisorbed species can be identified through a spectral decomposition. The first peak is observed at 161 ppm for both Mg−Al−15 and

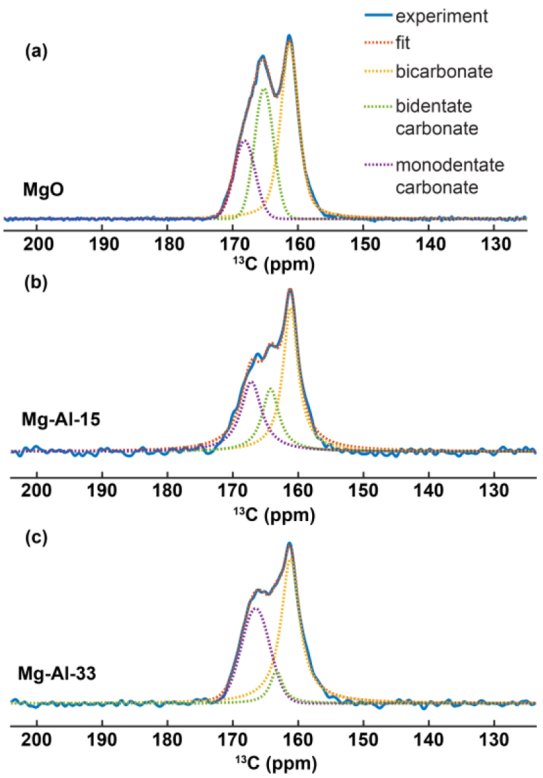

Figure 2. ^{1}H−^{13}C CP spectra of MgO (a) Mg−Al−15 (b) and Mg−Al−33 (c) dosed with $^{13}CO_2$ at 1 bar and 200 °C. Spectral deconvolution shows the components of the different chemisorbed products.

Mg−Al−33, and 2D ^{1}H−^{13}C HETCOR spectra (Figure 3) show a strong correlation of this peak to the bicarbonate proton at ^{1}H (~5.5 ppm). The bicarbonate ^{13}C and ^{1}H chemical shifts observed herein match the literature values of bicarbonate species in other MgO crystalline structures.[46,48] To confirm that this bicarbonate species was formed via chemisorption of CO_2 and not a residual product formed by the incomplete decomposition of the LDH starting material, SI Figure1 shows the ^{1}H quantitative NMR spectra before and after $^{13}CO_2$ adsorption. The clear formation of bicarbonate proton can be seen after the CO_2 adsorption at 5.5 ppm. IR measurements performed before and after calcination of the LDH material, (SI Figures 2 and 5) also confirmed the complete removal of the carbonate anion from the LDH upon calcination.

The other two spectroscopically resolved ^{13}C species are carbonate/MMOs species appearing at ^{13}C chemical shifts of 167.2 and 165.1 ppm in Mg−Al−15 and 166.5 and 163.3 ppm for Mg−Al−33. We assigned the higher ppm shifted carbonate species (167.2 and 166.5 ppm) to monodentate carbonate and the lower shifted carbonate peaks (165.1 and 163.3 ppm) to bidentate carbonate based on previous IR and NMR characterization[9,48] of heat-treated MgO, whereas the presence of multiple carbonate species formed upon CO_2 dosing at elevated temperatures was assigned to both mono- and bidentate carbonate species. In those studies, the reported ^{13}C chemical shift for the mono- and bidentate carbonate in MgO are 168 and 164 ppm, respectively, and agree well with those reported herein.

The 2D HETCOR spectrum of Mg−Al−15 shows that both the carbonate peaks correlate with a ^{1}H NMR peak centered at

https://doi.org/10.1021/acs.chemmater.1c03101
Chem. Mater. 2022, 34, 3893−3901

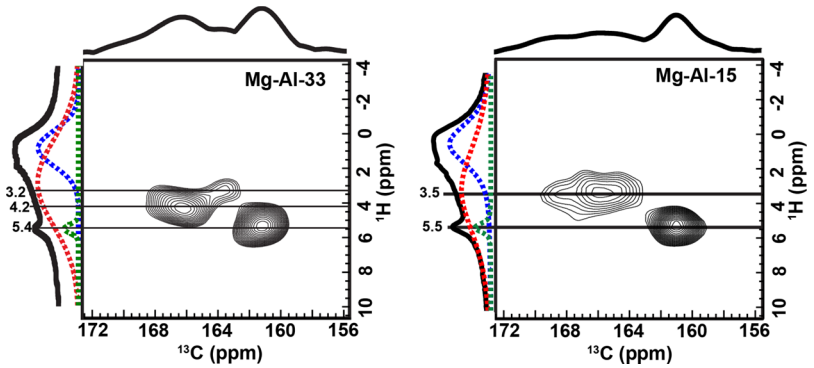

Figure 3. ^{1}H−^{13}C 2D HETCOR spectra of Mg−Al−33 (a) and Mg−Al−15 (b) using a mixing time of 200 μs and a spin rate of 10 kHz.

~3.5 ppm; this agrees well with the peak at 3.4 ppm in the ^{1}H quantitative spectra (as seen in the projection of the ^{1}H dimension in Figure 3). We attribute this broad correlation of the two carbonate species to the protons of mixed metal hydroxide MgAlOH. Studies of hydroxyl groups in Mg−Al LDHs with varying Al/Mg ratio from 0.19 to 0.33 showed the ^{1}H hydroxide group associated with the Al−Mg cluster range 2.9−4 ppm,[49] in good agreement with the broad proton resonance observed in the 2D HETCOR of the MMOs presented here and the quantitative ^{1}H spectra centered at 3.5 ppm.

The Mg−Al−33 carbonate species are correlated with broad proton resonances at 3.2 and 4.2 ppm; the latter increased proton shift is associated with the increased acidity of the mixed metal hydroxide group with increasing amounts of ^{27}Al in the material, as has been observed in the parent LDH material.[50] An additional peak is observed in the ^{1}H quantitative spectra for both Mg−Al−15 and Mg−Al−33 that is attributed to the hydroxyl group associated with the MgOH observed at a range of 0.9−0 ppm.[49−51] No correlation of the carbonated species was observed with these MgOH hydroxyl groups in the dosed MMOs. Thus, a combination of 1D and 2D ^{1}H−^{13}C NMR study of MMOs dosed with CO_2 at elevated temperatures leads us to the conclusion that there exist multiple chemisorbed products in the material—monodentate and bidentate carbonate and bicarbonate. The 2D HETCOR spectra of MMOs show that both the mono- and bidentate carbonate species are correlated to the mixed metal hydroxide, MgAlOH, likely due to an electrostatic interaction between the Al substitution site and the carbonate. The HETCOR establishes a proximity between the mono- and bidentate carbonate species and the Al substitution site. The exact role of MgAlOH protons in the material on carbonate formation is beyond the scope of this study.

Quantum Chemical Mechanistic Implications. We turn to quantum chemical calculations to further assess the formation of the carbonate and bicarbonate in the MMOs. Literature studies have proposed multiple CO_2 adsorption sites in the LDHs and the derived MMOs materials.[9,44,49] From these studies, multiple mechanisms have been proposed for the formation of CO_2 adsorption sites, such as the decomposition of active Mg−O species wherein the Al^{3+} substitutes for Mg^{2+} in the MgO lattice lead to coordinated unsaturated adjacent oxygen atoms that in turn becomes the basic sites for CO_2 chemisorption. Another proposed mechanism is the diffusion of Al out of the octahedral MgO layers leaving a vacancy site where the Mg−O active species is formed. We test these hypotheses by considering the DFT calculated ^{13}C chemical shifts of the chemisorbed CO_2 species adjacent to an Al^{3+} substitution site in the MMOs. Creating a reliable DFT model can be difficult, however, due to the complex atomic structure of the MMOs. Herein, we take the approach used previously[39,52] where cluster models are imagined to examine specific sites in the MMO material. The model system used for the simulations is based upon the cubic MgO structure.[38] Thus, these simulations are not to propose an exact structure for the MMO system but rather mimic the effect of site-specific substitution of Mg^{2+} with Al^{3+} on the ^{13}C chemical shifts of the chemisorbed species. Here we seek to discern which chemisorbed species are adjacent to Al sites by taking a corner Mg site in a MgO cubic cluster and substituting it with an Al atom as shown in Figure 4a,b. The ^{13}C chemical shift of either carbonate or bicarbonate species at the Mg corner site was then calculated with and without this Al substitution.

A comparison of the DFT and experimental NMR ^{13}C chemical shifts of the carbonate species is shown in Figure 4a. The experimental ^{13}C NMR isotropic chemical shift of the carbonate species decreases 1−2 ppm with increasing Al content: from 168 ppm in the decomposed MgO to 167.7 ppm in Mg−Al−15 and 166.5 ppm in Mg−Al−33 for the monodentate carbonate species and from 165.1 to 163.3 ppm for the bidentate carbonate species. The experimentally observed change in the isotropic shifts of 2 ppm with increasing Al content agrees well with DFT-calculated shifts of 167.2 ppm in the unsubstituted MgO cluster and 166.5 ppm with the Al substitution. This change in the ^{13}C isotropic chemical shift with Al substitution further demonstrates that both the mono- and bidentate carbonate species are more favorably formed at an Mg−O site with an adjacent Al substitution as opposed to isolated Mg−O sites.

For the *bicarbonate* species, the same analysis was performed, shown in Figure 4b, where the DFT calculation of the ^{13}C isotropic chemicals shift of bicarbonate in Mg−O are shown with and without an adjacent Al substitution. In contrast to the carbonate signal, increasing Al content does not show a significant change in the experimentally determined bicarbonate chemical shift (~ 161 ppm for all experimentally measured shifts). The DFT calculated chemical shifts for the unsubstituted and Al substituted bicarbonate species, however, shows a shift from 160.0 to 162.5 ppm, respectively. The unchanged experimentally determined bicarbonate ^{13}C chemical shift, regardless of Al content in the material, further supports our hypothesis that the bicarbonate species are formed from basic Mg_3OH sites and are not dependent on the Al substitution.

https://doi.org/10.1021/acs.chemmater.1c03101
Chem. Mater. 2022, 34, 3893−3901

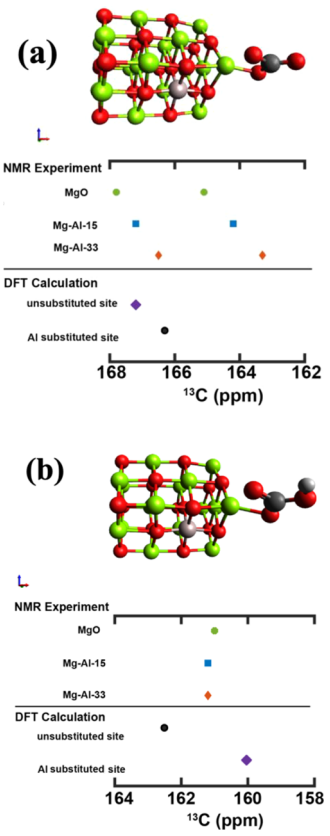

Figure 4. Comparison of experimentally measured and DFT calculated ^{13}C chemical shifts for the cubic MgO structure with and without adjacent Al substitution for carbonate (a) and bicarbonate (b). Mg (green), O (red), Al (light brown), C (dark gray), and H (light gray).

While the model system does estimate the effect of a single site Al substitution on carbon chemical shifts, this cluster is not representative of the actual Mg/Al ratios the MMO systems use here. We addressed this by randomly sampling carbonate and bicarbonate locations at 50 different Al positions in the cubical $Mg_{14}Al_4O_{18}$ system. The geometry was optimized and the resulting lowest energy configuration was used for the chemical shift calculation (Table 2). In structures with higher Al content, the carbonate species were located at oxygen atoms between two Mg with a large distortion in the cubic structure of the MMO. The large distortion in the cubic metal oxide structure with increasing Al content likely leads to the difference in chemical shift between the DFT ^{13}C chemical shift calculations and those determined experimentally.

This hypothesis is further supported by the consideration of the spatial proximity of Al to the bicarbonate moiety via ^{1}H−^{27}Al TRAPDOR, a methodology whereby rotationally refocused echoes of the ^{1}H spins during the MAS rotor period are interlaced with ^{27}Al excitation. During the first evolution period, continuous wave irradiation is applied to the ^{27}Al spins leading to the reintroduction of the dipolar interaction between proximate ^{1}H−^{27}Al pairs, causing a dephasing or reduced intensity of the ^{1}H species coupled to the ^{27}Al spin.[50,53] Figure 5 shows the refocused ^{1}H echoes with and without ^{27}Al irradiation and the difference between the two spectra. Here, normalization of the refocused echoes with and without irradiation considers signal reduction due to T_2, and error bars for each irradiation period were calculated from the signal-to-noise ratio of each echo spectrum. The difference spectra show a broad peak centered at 3.1 ppm attributed to the mixed metal hydroxyl groups, establishing the spatial correlation of these protons with aluminum ions. Importantly, the bicarbonate proton at 5.5 ppm is not affected by ^{27}Al irradiation. Figure 5b shows a plot of the $\Delta S/S_0$ values of the bicarbonate ^{1}H and mixed metal hydroxide showing that the bicarbonate proton remains largely undisturbed by ^{27}Al irradiation. The DFT simulations of the bicarbonate species formed at the MgO sites with an adjacent Al yield an approximate ^{1}H−^{27}Al distance of 6.8 Å, revealing that if the bicarbonate is formed at a Mg_2AlOH site the bicarbonate peak should exhibit a TRAPDOR dephasing effect. From the combination of the ^{13}C chemical shift calculations of the Mg−O carbonate with and without an adjacent Al site and the heteronuclear correlation data from TRAPDOR, we conclude that both the mono- and bidentate carbonate species preferentially form at the Mg−O sites with adjacent Al substitution. In contrast, the bicarbonate species are preferentially formed at the Mg−OH sites in the material without Al substitution, likely at basic Mg_3OH sites in the MMO material.

The Role of Al Content on CO_2 Capture Capacity. The CO_2 capture capacities of the MMOs were tested via gravimetric methods as detailed in the experimental section above and are given in Figure 6. The observed capture capacities were in the range of 0.45 to 0.82 mmol/g, where the 0.25 Al/Mg sample shows the highest CO_2 capture capacity of 0.82 mmol/g. These observations are in line with the literature-reported values for the LDH-derived MMOs.[44,54] For comparison, we also report the $Mg(OH)_2$-derived MgO CO_2 capture capacity of 1.36 mmol/g. While the initial capture capacity of the MgO is larger than the Al−Mg MMOs, it has been reported in the literature that the capture capacity drops off rapidly with the increasing number of cycles in the MgO material when compared with Al−Mg MMOs.[55]

To further address the role of Al, we quantitate the distribution of chemisorbed products formed after high-temperature CO_2 adsorption. We therefore analyzed the direct quantitative ^{13}C NMR spectra of CO_2 sorbed onto decomposed MgO, Mg−Al−15, and Mg−Al−33. These quantitative ^{13}C spectra were fit using the Dmfit software with a mixture of Gaussian and Lorentzian line shapes and the results of the spectral decompositions are summarized in Figure 7. The different carbonate and bicarbonate species form at a diverse range of basic sites in the MgO material with the bicarbonate formed at weakly basic MgOH sites, bidentate carbonate formed at medium basic sites, and monodentate carbonate forming at strongly basic sites.[48] The dominant chemisorbed product formed with $^{13}CO_2$ dosing at 200 °C on

Table 2. DFT Calculated ^{13}C Chemical Shifts (in ppm) of $Mg_{14}Al_4O_{18}$, $Mg_{17}AlO_{18}$, and MgO

	cubic $Mg_{14}A_4O_{18}$	cubic MgO w/Al substitution $Mg_{17}AlO_{18}$	cubic MgO $Mg_{18}O_{18}$
bicarbonate	160.5	162.5	160.0
carbonate	168.8	166.3	167.2

https://doi.org/10.1021/acs.chemmater.1c03101
Chem. Mater. 2022, 34, 3893−3901

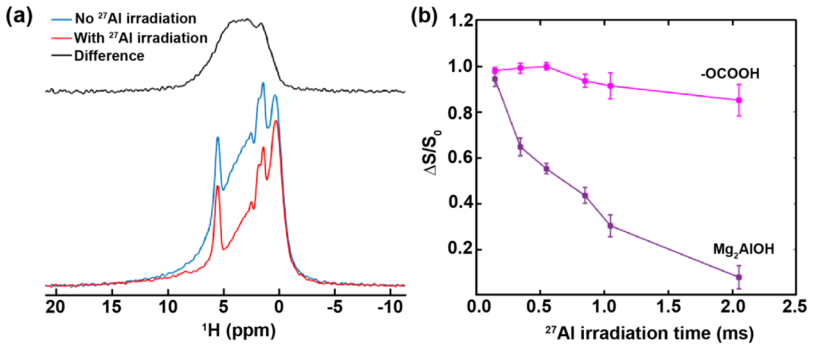

Figure 5. (a) TRAPDOR echo measurement of Mg−Al−15 at a proton frequency of 700 MHz and 10 kHz MAS. (b) $\Delta S/S_0$ of the spectral deconvolution as a function of ^{27}Al irradiation.

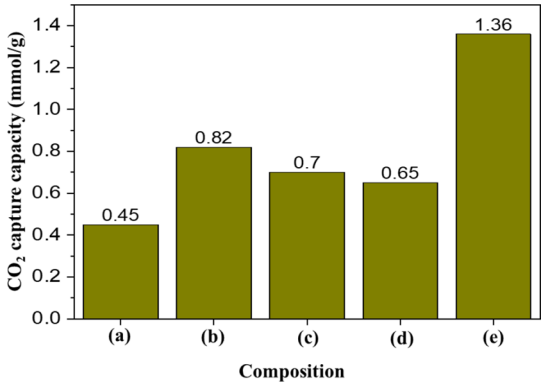

Figure 6. The CO_2 capture capacity (200 °C, 2 h, 90% CO_2) of MMOs generated from Mg−Al−CO_3 LDHs prepared by co-precipitation at pH 10 with varied Al/Mg ratios (a) 0.33, (b) 0.25, (c) 0.20, and (d) 0.15 and (e) $Mg(OH)_2$.

MgO is bidentate carbonate (49% of the NMR signal intensity), whereas 19% is associated with monodentate carbonate formation and 32% is associated with bicarbonate formation. This agrees with previous works that show that moderately basic sites are the predominant CO_2 adsorption sites in MgO, which form the bidentate carbonate chemisorbed product.[48]

The Mg−Al−15 MMO structure exhibits a 38% reduction in the bidentate carbonate component, while the monodentate carbonate signal increased to make up 28% and the bicarbonate species made up 34% of the chemisorbed product in the ^{13}C quantitative spectrum. As the Al content is increased further in Mg−Al−33 MMOs, the amount of bidentate carbonate is further reduced to 34% and the monodentate carbonate signal again increases to 34%, while the bicarbonate signal is also reduced to 32% of the total ^{13}C chemisorbed product. We find a general trend of a relative increase in monodentate carbonate signal with increasing Al content in these MMOs, consistent with the hypothesis that Al

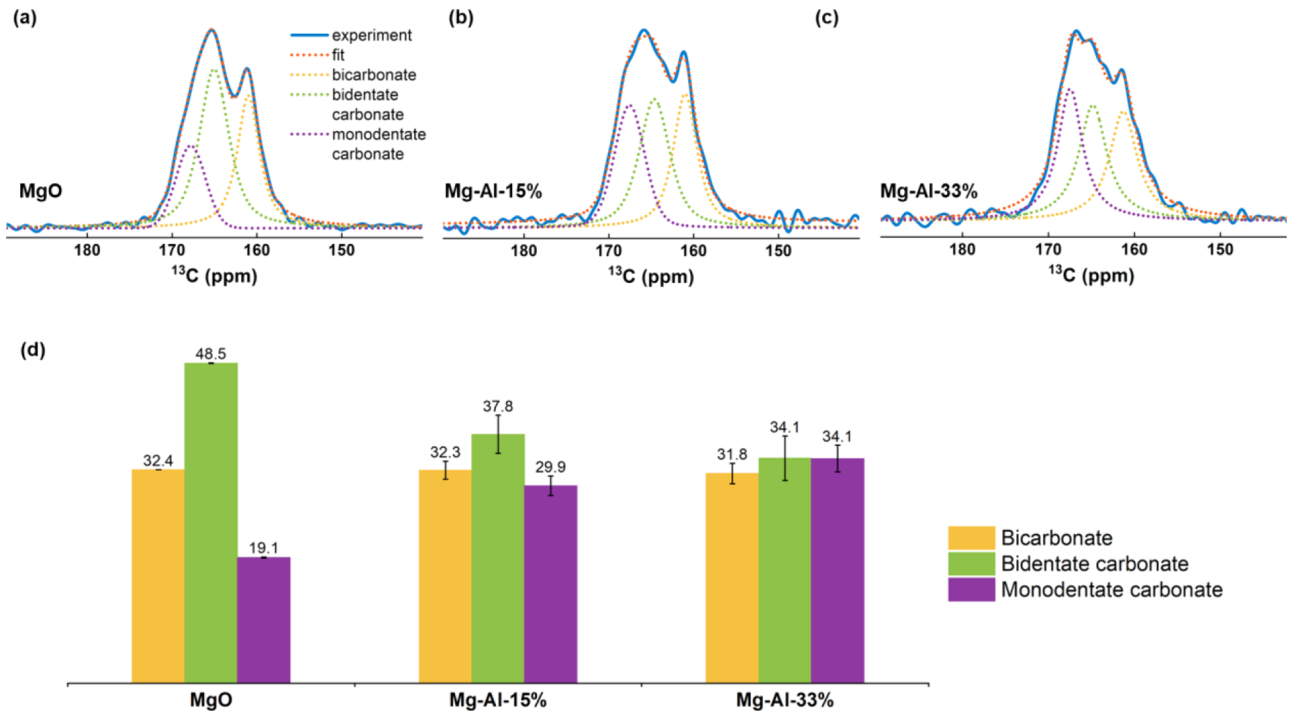

Figure 7. Quantitative ^{13}C NMR spectra $^{13}CO_2$ adsorbed onto MgO (a), Mg−Al−15 (b), and Mg−Al−33 (c). The integral percent of each chemisorbed species from the spectral decomposition is shown in (d).

https://doi.org/10.1021/acs.chemmater.1c03101
Chem. Mater. 2022, 34, 3893−3901

substitution creates strongly basic sites leading to a more favorable formation association of the monodentate carbonate species with these sites. In addition, this increase in the formation of strong basic Mg−O sites with increasing Al content appears to be also associated with the reduction of moderately basic sites in the material as evidenced by the decrease in the relative amount of bidentate carbonate sites with increasing Al content. The bicarbonate species are formed at the weak basic Mg−OH sites in the material, likely due to the calcination method causing partial dihydroxylation and removal of surface-bound water and thus showing only slight variation in the relative amount of Al content. With this context, we can examine the trend shown in Figure 6 where increasing Al from 0.15 to 0.25 molar shows a general trend of increase in the CO_2 capture capacity. Thus, one possibility for increasing the capacity would be to increase the relative amount of strongly basic sites in the MMO material. Increasing the Al content further to 0.33 shows a decrease in the CO_2 capture capacity of the MMO even upon further increasing the relative amount of strongly basic sites. This could be due to the drop in the absolute amount of adsorption sites available in the material; in addition, an increase in the Al content causes a decrease in the surface area of the MMO material, as measured by BET adsorption (SI Table 1). Finally, we characterized the Al structure in the material directly through ^{27}Al MQMAS NMR as detailed in SI Figures 10 and 11. The resulting isotropic shifts and quadrupolar parameters agree well with the previously reported values in the literature.[44,49,56,57]

CONCLUSIONS

The analysis of solid-state ^{13}C NMR spectra allows identification of mono- and bidentate carbonates and bicarbonates upon CO_2 adsorption onto Mg−Al MMOs. The comparison of DFT cluster calculations with changes in the ^{13}C chemical shift upon increasing the Al/Mg ratio supports the hypothesis that the mono- and bidentate carbonate species are formed at the Mg−Al mixed metal oxide sites, while the bicarbonate is formed at weakly basic Mg−OH sites. These calculations are confirmed via proton−aluminum double resonance measurements. Quantitative ^{13}C NMR spectra enumerate the ratios of chemisorbed species with increasing Al/Mg ratio and reveals that the relative amount of monodentate carbonate increases with increasing Al content, thus confirming the association of Al with strong basic sites in the MMOs. This detailed understanding of the various basic sites present in the MMO material and the formation of different chemisorbed species yields new insights into the mechanism of CO_2 adsorption. With this understanding of the CO_2 chemisorbed mechanism and further studies on the optimal synthesis and decomposition methods, we anticipate that increasing basic site availability without sacrificing surface area and capacity will afford the full potential of MMOs for CO_2 capture applications.

ASSOCIATED CONTENT

Supporting Information

The Supporting Information is available free of charge at https://pubs.acs.org/doi/10.1021/acs.chemmater.1c03101.

ICP analysis, PXRD and FTIR spectra, and TGA analysis of the synthesized Mg/Al LDHs, and the PXRD and FTIR spectra and N_2 adsorption isotherms of the MMOs generated from the Mg−AlCO_3 LDHs; Quantitative ^{1}H NMR and ^{27}Al MQMAS before and after $^{13}CO_2$ adsorption in MMOs; and the calculated energies of DFT simulations (PDF)

AUTHOR INFORMATION

Corresponding Author

Jeffrey A. Reimer − *Materials Science Division, Lawrence Berkeley National Laboratory, Berkeley, California 94720, United States; Department of Chemical and Biomolecular Engineering, University of California, Berkeley, California 94720, United States;* orcid.org/0000-0002-4191-3725; Email: reimer@berkeley.edu

Authors

Alicia Lund − *Materials Science Division, Lawrence Berkeley National Laboratory, Berkeley, California 94720, United States; Department of Chemical and Biomolecular Engineering, University of California, Berkeley, California 94720, United States;* orcid.org/0000-0001-7520-9544

G. V. Manohara − *Research Center for Carbon Solutions (RCCS), School of Engineering and Physical Sciences, Heriot-Watt University, Edinburgh EH14 4AS, U.K.*

Ah-Young Song − *Materials Science Division, Lawrence Berkeley National Laboratory, Berkeley, California 94720, United States; Department of Chemical and Biomolecular Engineering, University of California, Berkeley, California 94720, United States*

Kevin Maik Jablonka − *Laboratory of Molecular Simulation (LSMO), Institut des Sciences et Ingénierie Chimiques, École Polytechnique Fédérale de Lausanne (EPFL), Sion CH-1951, Switzerland;* orcid.org/0000-0003-4894-4660

Christopher P. Ireland − *Laboratory of Molecular Simulation (LSMO), Institut des Sciences et Ingénierie Chimiques, École Polytechnique Fédérale de Lausanne (EPFL), Sion CH-1951, Switzerland;* orcid.org/0000-0002-2436-3987

Li Anne Cheah − *Research Center for Carbon Solutions (RCCS), School of Engineering and Physical Sciences, Heriot-Watt University, Edinburgh EH14 4AS, U.K.*

Berend Smit − *Laboratory of Molecular Simulation (LSMO), Institut des Sciences et Ingénierie Chimiques, École Polytechnique Fédérale de Lausanne (EPFL), Sion CH-1951, Switzerland;* orcid.org/0000-0003-4653-8562

Susana Garcia − *Research Center for Carbon Solutions (RCCS), School of Engineering and Physical Sciences, Heriot-Watt University, Edinburgh EH14 4AS, U.K.;* orcid.org/0000-0002-3713-311X

Complete contact information is available at: https://pubs.acs.org/10.1021/acs.chemmater.1c03101

Notes

The authors declare no competing financial interest.
The DFT raw data is available at doi: 10.24435/materialscloud:ba-jz.

ACKNOWLEDGMENTS

The PrISMa Project (No. 299659) is funded through the ACT programme (Accelerating CCS Technologies, Horizon2020 Project No. 294766). Financial contributions made from the Department for Business, Energy & Industrial Strategy (BEIS) together with extra funding from the NERC and EPSRC research councils, United Kingdom; The Research Council of Norway, (RCN), Norway; the Swiss Federal Office of Energy

(SFOE), Switzerland; and the US-Department of Energy (US-DOE), USA, are gratefully acknowledged. Financial support from TOTAL and Equinor is also gratefully acknowledged. We thank Dr. Hasan Celik and UC Berkeley's NMR facility in the College of Chemistry (CoC-NMR) for spectroscopic assistance.

REFERENCES

(1) Smit, B.; Reimer, J. A.; Oldenburg, C. M.; Bourg, I. C. *Introduction to Carbon Capture and Sequestration*; Imperial College Press: London, UK, 2014.
(2) Smit, B.; Garcia, S. Carbon capture and storage: making fossil fuels great again? *Europhys. News* **2020**, *51*, 20−22.
(3) Bui, M.; Adjiman, C. S.; Bardow, A.; Boston, A.; Brown, S.; Fennell, P. S.; Fuss, S.; Galindo, A.; Hackett, L. A.; Hallett, J. P.; Herzog, H. J.; Jackson, G.; Kemper, J.; Krevor, S.; Maitland, G. C.; Matuszewski, M.; Metcalfe, I. S.; Petit, C.; Puxty, G.; Reimer, J.; Reiner, D. M.; Rubin, E. S.; Scott, S. A.; Shah, N.; Smit, B.; Trusler, J.; Webley, P.; Wilcox, J.; Dowell, N. M. Carbon capture and storage (CCS): The way forward. *Energy Environ. Sci.* **2018**, *11*, 1062−1176.
(4) Murge, P.; Dinda, S.; Roy, S. Zeolite-Based Sorbent for CO_2 Capture: Preparation and Performance Evaluation. *Langmuir* **2019**, *35*, 14751−14760.
(5) Saha, S.; Chandra, S.; Garai, B.; Banerjee, R. Carbon dioxide capture by metal organic frameworks. *Indian J. Chem.* **2012**, *51*, 1223−1230.
(6) Trickett, C. A.; Helal, A.; Al-Maythalony, B. A.; Yamani, Z. H.; Cordova, K. E.; Yaghi, O. M. The chemistry of metal-organic frameworks for CO_2 capture, regeneration and conversion. *Nat. Rev. Mater.* **2017**, *2*, 17045.
(7) An, S.; Xu, T.; Peng, C.; Hu, J.; Liu, H. Rational design of functionalized covalent organic frameworks and their performance towards CO_2 capture. *RSC Adv.* **2019**, *9*, 21438−21443.
(8) Wang, J.; Huang, H.; Wang, M.; Yao, L.; Qiao, W.; Long, D.; Ling, L. Direct capture of low-concentration CO_2 on mesoporous carbon-supported solid amine adsorbents at ambient temperature. *Ind. Eng. Chem. Res.* **2015**, *54*, 5319−5327.
(9) Gao, Y.; Zhang, Z.; Wu, J.; Yi, X.; Zheng, A.; Umar, A.; O'Hare, D.; Wang, Q. Comprehensive investigation of CO_2 adsorption on Mg-Al-CO_3 LDH-derived mixed metal oxides. *J. Mater. Chem. A* **2013**, *1*, 12782−12790.
(10) Sharma, U.; Tyagi, B.; Jasra, R. V. Synthesis and characterization of Mg-Al-CO_3 layered double hydroxide for CO_2 adsorption. *Ind. Eng. Chem. Res.* **2008**, *47*, 9588−9595.
(11) Ram Reddy, M. K.; Xu, Z. P.; Lu, G. Q.; Da Costa, J. C. D. Layered double hydroxides for CO_2 capture: Structure evolution and regeneration. *Ind. Eng. Chem. Res.* **2006**, *45*, 7504−7509.
(12) Flores-Granobles, M.; Saeys, M. Minimizing CO_2 emissions with renewable energy: A comparative study of emerging technologies in the steel industry. *Energy Environ. Sci.* **2020**, *13*, 1923−1932.
(13) Van Dijk, H. A. J.; Cobden, P. D.; Lukashuk, L.; Water, L. V.; Lundqvist, M.; Manzolini, G.; Cormos, C.; van Dijk, C.; Mancuso, L.; Johns, J.; Bellqvist, D. Stepwise project: Sorption-enhanced water-gas shift technology to reduce carbon footprint in the iron and steel industry. *Johnson Matthey Technol. Rev.* **2018**, *62*, 395−402.
(14) Cavani, F.; Trifirò, F.; Vaccari, A. Hydrotalcite-type anionic clays: Preparation, properties and applications. *Catal. Today* **1991**, *11*, 173−301.
(15) Li, C.; Wei, M.; Evans, D. G.; Duan, X. Layered double hydroxide-based nanomaterials as highly efficient catalysts and adsorbents. *Small* **2014**, *10*, 4469−4486.
(16) Panda, H. S.; Srivastava, R.; Bahadur, D. In-vitro release kinetics and stability of anticardiovascular drugs-intercalated layered double hydroxide nanohybrids. *J. Phys. Chem. B* **2009**, *113*, 15090−15100.
(17) Theiss, F. L.; Ayoko, G. A.; Frost, R. L. Iodide removal using LDH technology. *Chem. Eng. J.* **2016**, *296*, 300−309.
(18) Ram Reddy, M. K.; Xu, Z. P.; Lu, G. Q.; Diniz Da Costa, J. C. Influence of water on high-temperature CO_2 capture using layered double hydroxide derivatives. *Ind. Eng. Chem. Res.* **2008**, *47*, 2630−2635.
(19) Ramírez-Moreno, M. J.; Romero-Ibarra, I. C.; Hernández-Pérez, M. A.; Pfeiffer, H. CO_2 adsorption at elevated pressure and temperature on Mg-Al layered double hydroxide. *Ind. Eng. Chem. Res.* **2014**, *53*, 8087−8094.
(20) Wang, Q.; Tay, H. H.; Zhong, Z.; Luo, J.; Borgna, A. Synthesis of high-temperature CO_2 adsorbents from organo-layered double hydroxides with markedly improved CO_2 capture capacity. *Energy Environ. Sci.* **2012**, *5*, 7526−7530.
(21) Wang, J.; Zhang, Y.; Altaf, N.; O'Hare, D.; Wang, Q. CHAPTER 1. Layered Double Hydroxides-derived Intermediate-temperature CO_2 Adsorbents. In *Pre-combustion Carbon Dioxide Capture Materials*; Inorganic Materials Series, Wang, Q.; The Royal Society of Chemistry, 2018; pp 1−60, DOI: 10.1039/9781788013390-00001.
(22) Van Dijk, E.; Walspurger, S.; Cobden, P.; Van Den Brink, R. Testing of hydrotalcite based sorbents for CO_2 and H_2S capture for use in sorption enhanced water gas shift. *Energy Procedia* **2011**, *4*, 1110−1117.
(23) Singh, R.; Ram Reddy, M. K.; Wilson, S.; Joshi, K.; Diniz da Costa, J. C.; Webley, P. High temperature materials for CO_2 capture. *Energy Procedia* **2009**, *1*, 623−630.
(24) Manohara, G. V.; Maroto-Valer, M. M.; Garcia, S. The effect of the layer-interlayer chemistry of LDHs on developing high temperature carbon capture materials. *Dalton Trans.* **2020**, *49*, 923−931.
(25) Manohara, G. V. Exfoliation of layered double hydroxides (LDHs): A new route to mineralize atmospheric CO_2. *RSC Adv.* **2014**, *4*, 46126−46132.
(26) Wong, Y. T. A.; Martins, V.; Lucier, B. E. G.; Huang, Y. Solid-State NMR Spectroscopy: A Powerful Technique to Directly Study Small Gas Molecules Adsorbed in Metal−Organic Frameworks. *Chem. − Eur. J.* **2019**, *25*, 1848−1853.
(27) Lucier, B. E. G.; Chan, H.; Zhang, Y.; Huang, Y. Multiple Modes of Motion: Realizing the Dynamics of CO Adsorbed in M-MOF-74 (M = Mg, Zn) by Using Solid-State NMR Spectroscopy. *Eur. J. Inorg. Chem.* **2016**, 2017−2024.
(28) Werner, M.; Rothermel, N.; Breitzke, H.; Gutmann, T.; Buntkowsky, G. Recent Advances in Solid State NMR of Small Molecules in Confinement. *Isr. J. Chem.* **2014**, *54*, 60−73.
(29) Milner, P. J.; Siegelman, R. L.; Forse, A. C.; Gonzalez, M. I.; Runčevski, T.; Martell, J. D.; Reimer, J. A.; Long, J. R. A Diaminopropane-Appended Metal-Organic Framework Enabling Efficient CO_2 Capture from Coal Flue Gas via a Mixed Adsorption Mechanism. *J. Am. Chem. Soc.* **2017**, *139*, 13541−13553.
(30) Forse, A. C.; Milner, P. J.; Lee, J.; Redfearn, H. N.; Oktawiec, J.; Siegelman, R. L.; Martell, J. D.; Dinakar, B.; Zasada, L. B.; Gonzalez, M. I.; Neaton, J. B.; Long, J. R.; Reimer, J. A. Elucidating CO_2 Chemisorption in Diamine-Appended Metal−Organic Frameworks. *J. Am. Chem. Soc.* **2018**, *140*, 18016−18031.
(31) Marti, R. M.; Howe, J. D.; Morelock, C. R.; Conradi, M. S.; Walton, K. S.; Sholl, D. S.; Hayes, S. E. CO_2 dynamics in pure and mixed-metal MOFs with open metal sites. *J. Phys. Chem. C* **2017**, *121*, 25778−25787.
(32) Wittmann, T.; Tschense, C. B. L.; Zappe, L.; Koschnick, C.; Siegel, R.; Stäglich, R.; Lotsch, B. V.; Senker, J. Selective host-guest interactions in metal-organic frameworks: Via multiple hydrogen bond donor-acceptor recognition sites. *J. Mater. Chem. A* **2019**, *7*, 10379−10388.
(33) Nielsen, U. G. Solid state NMR studies of photoluminescent. *Annu. Rep. NMR Spectrosc.* **2021**, *104*, 75−140.
(34) Massiot, D.; Fayon, F.; Capron, M.; King, I. J.; Le Calvé, S.; Alonso, B.; Durand, J.; Bujoli, B.; Gan, Z.; Hoatson, G. L. Modelling one- and two-dimensional solid-state NMR spectra. *Magn. Reson. Chem.* **2002**, *40*, 70−76.
(35) Cory, D. G.; Ritchey, W. M. Suppression of signals from the probe in bloch decay spectra. *J. Magn. Reson.* **1988**, *80*, 128−132.

(36) Bielecki, A.; Kolbert, A. C.; Levitt, M. H. Frequency-switched pulse sequences: Homonuclear decoupling and dilute spin NMR in solids. *Chem. Phys. Lett.* **1989**, *155*, 341−346.
(37) Amoureux, J. P.; Fernandez, C.; Steuernagel, S. Z Filtering in MQMAS NMR. *J. Magn. Reson., Ser. A* **1996**, *123*, 116−118.
(38) Wobbe, M. C. C.; Kerridge, A.; Zwijnenburg, M. A. Optical excitation of MgO nanoparticles; a computational perspective. *Phys. Chem. Chem. Phys.* **2014**, *16*, 22052−22061.
(39) Bawa, F.; Panas, I. Limiting properties of $(MgO)_n$ and $(CaO)_n$ clusters. *Phys. Chem. Chem. Phys.* **2001**, *3*, 3042−3047.
(40) Krishnan, R.; Binkley, J. S.; Seeger, R.; Pople, J. A. Self-consistent Molecular Orbital Methods. XX. A Basis Set for Correlated Wave Functions. *J. Chem. Phys.* **1980**, *72*, 650−654.
(41) Huber, S. P.; Zoupanos, S.; Uhrin, M.; Talirz, L.; Kahle, L.; Häuselmann, R.; Gresch, D.; Müller, T.; Yakutovich, A. V.; Andersen, C. W.; Ramirez, F. F.; Adorf, C. S.; Gargiulo, F.; Kumbhar, S.; Passaro, E.; Johnston, C.; Merkys, A.; Cepellotti, A.; Mounet, N.; Marzari, N.; Kozinsky, B.; Pizzi, G. AiiDA 1.0, a scalable computational infrastructure for automated reproducible workflows and data provenance. *Sci. Data* **2020**, *7*, 300.
(42) Frisch, M. J.; Trucks, G. W.; Schlegel, H. B.; Scuseria, G. E.; Robb, M. A.; Cheeseman, J. R.; Scalmani, G.; Barone, V.; Petersson, G. A.; Nakatsuji, H.; Li, X.; Caricato, M.; Marenich, A. V.; Bloino, J.; Janesko, B. G.; Gomperts, R.; Mennucci, B.; Hratchian, H. P.; Ortiz, J. V.; Izmaylov, A. F.; Sonnenberg, J. L.; Williams-Young, D.; Ding, F.; Lipparini, F.; Egidi, F.; Goings, J.; Peng, B.; Petrone, A.; Henderson, T.; Ranasinghe, D.; Zakrzewski, V. G.; Gao, J.; Rega, N.; Zheng, G.; Liang, W.; Hada, M.; Ehara, M.; Toyota, K.; Fukuda, R.; Hasegawa, J.; Ishida, M.; Nakajima, T.; Honda, Y.; Kitao, O.; Nakai, H.; Vreven, T.; Throssell, K.; Montgomery, J. A., Jr.; Peralta, J. E.; Ogliaro, F.; Bearpark, M. J.; Heyd, J. J.; Brothers, E. N.; Kudin, K. N.; Staroverov, V. N.; Keith, T. A.; Kobayashi, R.; Normand, J.; Raghavachari, K.; Rendell, A. P.; Burant, J. C.; Iyengar, S. S.; Tomasi, J.; Cossi, M.; Millam, J. M.; Klene, M.; Adamo, C.; Cammi, R.; Ochterski, J. W.; Martin, R. L.; Morokuma, K.; Farkas, O.; Foresman, J. B.; Fox, D. J. *Gaussian 16, Revision C.01*; Gaussian, Inc.: Wallingford CT, 2016.
(43) Wolinski, K.; Hinton, J. F.; Pulay, P. Efficient Implementation of the Gauge-Independent Atomic Orbital Method for NMR Chemical Shift Calculations. *J. Am. Chem. Soc.* **1990**, *112*, 8251−8260.
(44) Sahoo, P.; Ishihara, S.; Yamada, K.; Deguchi, K.; Ohki, S.; Tansho, M.; Shimizu, T.; Eisaku, N.; Sasai, R.; Labuta, J.; Ishikawa, D.; Hill, J. P.; Ariga, K.; Bastakoti, B. P.; Yamauchi, Y.; Iyi, N. Rapid Exchange between Atmospheric CO_2 and Carbonate Anion Intercalated within Magnesium Rich Layered Double Hydroxide. *ACS Appl. Mater. Interfaces* **2014**, *6*, 18352−18359.
(45) Fu, Y.; Zhang, L.; Yue, B.; Chen, X.; He, H. Simultaneous Characterization of Solid Acidity and Basicity of Metal Oxide Catalysts via the Solid-State NMR Technique. *J. Phys. Chem. C* **2018**, *122*, 24094−24102.
(46) Moore, J. K.; Surface, J. A.; Brenner, A.; Skemer, P.; Conradi, M. S.; Hayes, S. E. Quantitative Identification of Metastable Magnesium Carbonate Minerals by Solid-State ^{13}C NMR Spectroscopy. *Environ. Sci. Technol.* **2015**, *49*, 657−664.
(47) Cui, J.; Olmsted, D. L.; Mehta, A. K.; Asta, M.; Hayes, S. E. NMR Crystallography: Evaluation of Hydrogen Positions in Hydromagnesite by $^{13}C\{^1H\}$ REDOR Solid-State NMR and Density Functional Theory Calculation of Chemical Shielding Tensors. *Angew. Chem., Int. Ed.* **2019**, *58*, 4210.
(48) Gao, W.; Zhou, T.; Wang, Q. Controlled synthesis of MgO with diverse basic sites and its CO_2 capture mechanism under different adsorption conditions. *Chem. Eng. J.* **2018**, *336*, 710−720.
(49) Sideris, P. J.; Blanc, F.; Gan, Z.; Grey, C. P. Identification of Cation Clustering in Mg−Al Layered Double Hydroxides Using Multinuclear Solid State Nuclear Magnetic Resonance Spectroscopy. *Chem. Mater.* **2012**, *24*, 2449−2461.
(50) Sideris, P. J.; Nielsen, U. G.; Gan, Z.; Grey, C. P. Mg/Al Ordering in Layered Double Hydroxides Revealed by Multinuclear NMR Spectroscopy. *Science* **2008**, *321*, 113−117.
(51) Mi, J.; Chen, X.; Zhang, Q.; Zheng, Y.; Xiao, Y.; Liu, F.; Aua, C.; Jiang, L. Mechanochemically synthesized MgAl layered double hydroxide nanosheets for efficient catalytic removal of carbonyl sulfide and H_2S. *Chem. Commun.* **2019**, *55*, 9375−9378.
(52) Rugg, G.; Genest, A.; Rö, N. DFT Variants for Mixed-Metal Oxides. Benchmarks Using Multi-Center Cluster Models. *J. Phys. Checm. A* **2018**, *122*, 7042−7050.
(53) Grey, C. P.; Vega, A. J. Determination of the Quadrupole Coupling Constant of the Invisible Aluminum Spins in Zeolite HY with $^1H/^{27}A1$ TRAPDOR NMR. *J. Am. Chem. Soc.* **1995**, *117*, 8232−8242.
(54) Radha, S.; Navrotsky, A. Energetics of CO_2 Adsorption on Mg−Al Layered Double Hydroxides and Related Mixed Metal Oxides. *J. Phys. Chem. C* **2014**, *118*, 29836−29844.
(55) Nityashree, N.; Manohara, G. V.; Maroto-Valer, M. M.; Garcia, S. Advanced High-Temperature CO_2 Sorbents with Improved Long-Term Cycling Stability. *ACS Appl. Mater. Interfaces* **2020**, *12*, 33765−33774.
(56) Vyalikh, A.; Massiot, D.; Scheler, U. Structural characterisation of aluminium layered double hydroxides by ^{27}Al solid-state NMR. *Solid State Nucl. Magn. Reson.* **2009**, *36*, 19−23.
(57) d'Espinose de Lacaillerie, J.-B.; Fretigny, C.; Massiot, D. MAS NMR spectra of quadrupolar nuclei in disordered solids: the Czjzek model. *J. Magn. Reson.* **2008**, *192*, 244−251.

https://doi.org/10.1021/acs.chemmater.1c03101
Chem. Mater. 2022, 34, 3893−3901